Suitability of Gelatin Methacrylate and Hydroxyapatite Hydrogels for 3D Bioprinted Bone Tissue

Paul Stolarov , Jonathan De Vries , Sean Stapleton , Lauren Morris , Kari Martyniak , Thomas Kean *

Posted Date: 27 December 2023

doi: 10.20944/preprints202312.2084.v1

Keywords: 3D Bioprinting; Hydroxyapatite; GelMA; Bone; DoE; Design of Experiments; bone bioprinting

Article

Suitability of Gelatin Methacrylate and Hydroxyapatite Hydrogels for 3D Bioprinted Bone Tissue

Paul Stolarov, Jonathan de Vries, Sean Stapleton, Lauren Morris, Kari Martyniak and Thomas J. Kean *

Biionix Cluster, Internal Medicine, College of Medicine, University of Central Florida, Orlando, FL
* Correspondence: thomas.kean@ucf.edu

Abstract: Background: Complex bone defects are challenging to treat. Autografting is the gold standard for regenerating bone defects, however limitations include donor site morbidity and increased surgical complexity. Advancements in 3D bioprinting (3DBP) offer a promising alternative for viable bone grafts. Methods: Design of Experiments (DoE) was used to design 12 hydrogel bioinks of various Gelatin methacrylate/hydroxyapatite (GelMA/HA) concentrations. These bioinks were assessed for pipettability and equilibrium modulus. An optimal bioink was designed using the DoE data to produce the greatest stiffness while still being pipettable. Two bioinks, the DoE designed maximal stiffness and the experimentally defined maximal stiffness vs. a literature based control were then printed using a 3D bioprinter and assessed for print fidelity. The resulting hydrogels were combined with human bone-marrow-derived mesenchymal stromal cells (hMSCs) and evaluated for cell viability. Results: DoE ANOVA analysis indicated that the augmented 3 level factorial design model used was a good fit ($p < 0.0001$). Using the model, DoE correctly predicted that a composite hydrogel consisting of 12.3% GelMA, 15.7% HA, and 2% Gelatin would produce the maximum equilibrium modulus while still being pipettable. The hydrogel with the most optimal print fidelity was 10% GelMA, 2% HA, and 5% Gelatin. There were no significant differences in cell viability within hydrogels from day 2 to day 7 ($p > 0.05$). There was however a significantly lower cell viability in the gel composed of 12.3% GelMA, 15.7% HA, and 2% gelatin compared to the other gels with lower HA concentration ($p < 0.05$), showing that higher HA or print pressure may be cytotoxic within hydrogels. Conclusions: Extrusion-based 3DBP offers significant advantages for bone-tissue implants due to its high customizability. This study demonstrates it is possible to create printable bone-like grafts from GelMA and HA with increased HA levels, favorable mechanical properties (145kPa) and >80% cell viability.

Keywords: 3D Bioprinting; Hydroxyapatite; GelMA; Bone; DoE; Design of Experiments

1. Introduction:

Bone is a versatile tissue that has a significant capacity for regeneration. However, the successful regeneration of complex bone defects is currently one of the biggest challenges faced by reconstructive surgeons [1]. Smaller bone defects can usually heal without intervention, as is the case with many types of fractures and small cranial bone defects [2]. Large or complex defects, termed critical-sized defects, exceed the natural capacity for regeneration, requiring further intervention [2]. Currently, the most common methods used for repairing large bone defects are autografting (transplanting bone from another site on a single patient) and allografting (transplanting cadaver bone) [2]. These structures are often hand-carved to fit the size of the defect [2]. Despite being considered the current gold standard, autografting and allografting are associated with significant drawbacks. Autografting can lead to donor site morbidity and requires more complex surgery. Allografting may be limited by the supply of donors, the potential for immunogenicity, and the risk

 doi:10.20944/preprints202312.2084.v1

of disease transmission [1]. Although conflicts of interest should be noted, studies on cell-infused cellular bone matrices have shown high success rates and low complication rates in spinal fusion [3].

In the past decade, tissue engineering of bone through 3-Dimensional Bioprinting (3DBP) has emerged as a possible solution for the challenges associated with bone autografting and allografting [4]. 3DBP is the fabrication of a tissue-like construct through the deposition of living cells often suspended in a hydrogel. When the cells and hydrogel are combined, they make up a liquid "bioink" that can be extruded from a bioprinter in layers to produce a cellular scaffold [5,6]. This scaffold can be subjected to covalent photocrosslinking during or after printing, producing a hardened construct that resembles the bone microenvironment. A significant advantage of 3DBP over allografting and autografting is that patient-derived autologous mesenchymal stromal cells (hMSCs) could be used in the construct, reducing the potential for graft immunogenicity and donor site morbidity. Additional advantages of 3DBP over allografting are decreased risk of infection, the ability to easily create large complex shapes, and the use of organic and biological additives to aid osteogenesis [5,7].

A significant challenge in 3DBP bone-like constructs is formulating a bioink that closely mimics the bone microenvironment. Natural bone is typically 20-40% collagen, 60-80% mineral, and 10-20% water [8]. The young's modulus of cortical and trabecular bone is ~19.9 GPa and ~18.0 GPa, respectively [9]. While the modulus of pre-calcified bone matrix housing bone marrow is around 64 kPa [10]. Bone bioinks currently used for 3DBP generally consist of three components: the base material, living cells, and various natural or synthetic additives. The base materials (most commonly alginate, gelatin methacrylate, or hyaluronic acid) in the bioink can be cross-linked after printing to increase the mechanical stiffness of the construct significantly [7,11].

Gelatin (a hydrolyzed product of collagen) with methacryloyl side groups (GelMA) is a popular base material in bone 3DBP because of its ability to be cross-linked in the presence of a photoinitiator [12–14]. Low concentrations of pure GelMA (5% w/v) can be extruded more easily and generate higher cell viability [15]. However, low concentrations of GelMA lack the stiffness needed to produce a construct that resembles the rigidity and load-bearing capacity of bone. Higher concentrations of GelMA (15% w/v) require higher pressure to be extruded and may decrease cell viability, although this can be overcome by warming the material to a liquid before extrusion [15]. To maximize printability and cell viability, most groups have used GelMA concentrations between 5% and 15% w/v for 3DBP [7]. In addition, low concentrations of pure gelatin can be added to GelMA hydrogels to increase the viscosity and printability of the material, without significantly affecting the material characteristics [16].

Natural and synthetic additives such as hydroxyapatite, bioactive glass, and graphene oxide have a significant impact on the structural stability of a bioink [17]. Additives can also increase cell viability within the hydrogel in low concentrations and promote differentiation into target tissues like bone or cartilage [18]. Hydroxyapatite (HA) is the primary inorganic material found in bone tissue which makes it a desirable additive for bone tissue engineering [17]. When used as an additive with pure gelatin hydrogels, HA has been shown to improve the mechanical stiffness of engineered bone tissue by up to 70% (42 kPa to 72 kPa) [19]. However, higher concentrations of HA may decrease cell viability due to its high calcium content [20].

Some of the most important characteristics of a bioprinted structure are printability, print fidelity, mechanical strength, and cell viability [21]. Printability, also called extrudability in extrusion bioprinting, is defined as the printing parameters necessary to print a straight line of defined width. Printability is influenced by pressure, temperature, speed, acceleration, and the diameter of the needle used for printing [21]. Determining printability is an important step in evaluating the feasibility of printing a bioink. Print fidelity is the degree to which the bioprinted structure holds its shape and it is related to the viscosity of the bioink [22]. 3D bioprinted structures often require a high print fidelity and it is crucial to balance print fidelity with printability to enable custom, defect-specific implants based on high resolution clinical imaging [7]. The mechanical stiffness of the printed product is particularly important as bioprinted bone structures should have significant load-bearing capabilities to maximize bone healing when implanted [23]. Mechanical properties can be determined by stress-testing the material. In this study we will calculate the equilibrium modulus to determine

 doi:10.20944/preprints202312.2084.v1

the mechanical properties of the materials [24]. Lastly, the high pressures and cross-linking procedures required for 3DBP bone tissues with high mechanical strength can have a deleterious effect on cell viability [15]. Evaluating the viability of human cells in each printable bioink after the printing process is an important step in determining their suitability as bone replacement implants.

A previous study used GelMA and HA for 3DBP and determined that the addition of HA in low concentrations (≤2%) to a 10% GelMA hydrogel maintained equal cell viability and decreased hydrogel swelling in comparison to constructs without HA [25]. The ideal combination of these materials for optimizing printability, print fidelity, mechanical strength, and cell viability remains largely unknown.

Testing bioprinting with a wide range of material concentrations with more than one material is challenging. Design of Experiments software (DoE) can aid in the experimental planning and analysis [13,14,26]. The software allows researchers to determine optimal values for further testing from fewer experiments based on desired outcomes.

For example, if the software is given maximum and minimum values of two material concentrations within a hydrogel, it will determine a subset of combinations within that range that will produce the greatest coverage of the design space with the fewest runs in an experiment. After the experiment, the results can be analyzed by the software, which can then predict the ideal concentrations of both materials in a hydrogel for a desired outcome [13,14,26].

The objective of this study was therefore to determine the ideal GelMA/HA bioink combination with added gelatin for extrusion-based 3DBP of bone-like constructs laden with hMSCs. To accomplish this, we experimentally evaluated the effects of various combinations of GelMA and HA with 2% Gelatin on printability, print fidelity, mechanical properties, and cell viability.

We hypothesized there would be a direct relationship between GelMA/HA concentrations and equilibrium modulus, but an inverse relationship between GelMA/HA concentrations and printability, print fidelity, and cell viability.

2. Materials and Methods

2.1. Cell Culture

Human bone-marrow-derived mesenchymal stromal cells (hMSCs) were thawed at passage 2 from a frozen stock of hMSCs isolated under Institutional Review Board-approved non-human research protocols (University of Central Florida College of Medicine STUDY00001124) and cultured until passage 5, at which point the experiments were performed. The cells were cultured in growth medium containing Dulbecco's Modified Eagle Medium (DMEM; Gibco Inc.) supplemented with 10% fetal bovine serum (FBS, Atlanta Biologicals Inc.), and 1% penicillin/streptomycin (Gibco). The cells were incubated in a humidified environment at 37°C with 5% CO_2. At ~90% confluence, the cells were trypsinized (0.25% trypsin/EDTA, Gibco), neutralized with growth media, centrifuged (500 RCF, 5 min), and resuspended in growth media. Live cells were counted (Cytosmart) using trypan blue exclusion. Cells were combined with the bioinks at a final concentration of ~1 x 10^6 cells/mL.

2.2. Design of Experiments Parameters

Experimental design software (DesignExpert, StatEase Inc.) was utilized to determine the hydrogel formulations for testing based on GelMA concentrations between 5% and 15% w/v and HA concentrations between 1% and 33%. The software produced 17 experimental runs with various GelMA/HA bioink formulations at 2% Gelatin, some of which are repeated to test experimental variability (Table 1).

The 17 hydrogels were first assessed based on their pipettability and equilibrium modulus of a cast cylinder. The bioinks with the ideal printability and mechanical properties were later 3D bioprinted and evaluated for their print fidelity and cell viability.

 doi:10.20944/preprints202312.2084.v1

Table 1. Initial Bioink Formulations.

Bioink designation	GelMA (%)	HA (%)	Gelatin (%)
G5H1	5	1	2
G5H17	5	17	2
G5H33	5	33	2
G7.5H9A	7.5	9	2
G7.5H9B	7.5	9	2
G7.5H25	7.5	25	2
G10H1	10	1	2
G10H17A	10	17	2
G10H17B	10	17	2
G10H17C	10	17	2
G10H33	10	33	2
G12.5H9	12.5	9	2
G12.5H25A	12.5	25	2
G12.5H25B	12.5	25	2
G15H1	15	1	2
G15H17	15	17	2
G15H33	15	33	2

Bioinks with A, B or C following them are replicates of the same composition.

2.3. Bioink formulation

The 17 experimental bioinks (Table 1) were prepared using GelMA at a methacrylation level of 45-55% (Rousselot Inc.) in PBS containing 0.05% lithium phenyl-2,4,6-trimethyl-benzoyl phosphinate (LAP) as the photoinitiator (Cellink Inc.) with 2% 300 bloom Gelatin (Electron Microscopy Sciences Inc.). The solution was warmed at 37°C on a hot plate and vortexed at 1500 revolutions per minute until dissolved. Various concentrations of HA powder (Sigma-Aldrich) were added to the solution and stirred until suspended. The hydrogel was combined with the cultured hMSCs at a concentration of ~1x10^6 cells/mL [27].

2.4. Printability

For the purposes of this study, printability was defined as the ability of a material to be pipetted and extruded as a gel at a temperature under 37 °C. A 0.2 mL sample of each of the 17 composite hydrogels (no cells) was warmed to 37 °C and pipetted. Bioinks that could not be pipetted or extruded were deemed unprintable. A composite score was developed for each bioink from the results, where printability is a dichotomous variable (1 = printable, 0 = not printable).

2.5. Mechanical testing

Mechanical testing was performed using a TA.XTPlusC mechanical testing device (Stable Micro Systems Inc.). Each of the 17 acellular composite hydrogels were heated to 37°C and pipetted into circular casts made using a biopsy punch in a silicone mat giving discs 5 mm in diameter by 0.5 mm in height. The discs and casts were held with a microscope slide and coverslip. They were then photo-crosslinked using a 300mW laser with visible light at 405 nm (Luck Laser Inc.). The laser was positioned 3.5cm above the hydrogels which were treated on both sides for 60 seconds.

A Texture-Analyzer 12.7 mm diameter cylindrical probe (TA-10) with a 5kg load cell was used for compression. Uniaxial compression was initiated at a speed of 0.1 mm/s and trigger force of 0.1g. Cylinders were compressed to 5, 10, 15, 20 and 25% strain and allowed to equilibrate for 5, 10, 15, 30 and 45 mins respectively. The materials were tested at room temperature in PBS. The output was plotted using the Exponent Connect software (Stable Micro Systems Inc.) to produce the force/time curve. The slope of the curve fitted to those stress/strain points was taken as the equilibrium modulus.

 doi:10.20944/preprints202312.2084.v1

2.6. Bioprinting

Bioprinting was performed with a BioAssemblyBot 3D bioprinter (Advanced Solutions Inc.) using pneumatic extrusion bioprinting (Figure 1). Each bioink was loaded into a disposable, UV-blocking amber cartridge (Nordson Inc.) with 20-gauge 0.5 inch straight needle dispensing tips (Nordson Inc.). Tissue Structure Information Modeling (TSIM, Advanced Solutions Inc.) software was used for 3D modeling. After printing, constructs were photo-crosslinked using a 200mW laser and visible light at 405nm positioned 3.5cm above the construct (Luck Laser Inc.).

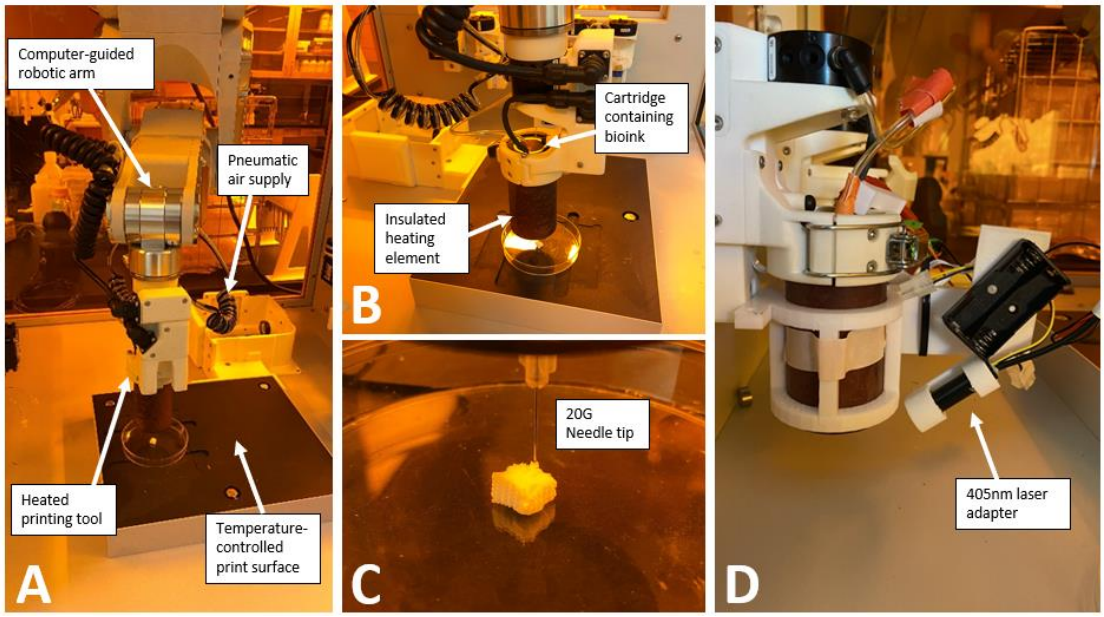

Figure 1. Bioprinter Assembly. (A) BioAssemblyBot 3D bioprinter by Advanced Solutions Inc. (B) Cartridges containing the bioinks were inserted into the heating tool and allowed to warm to the desired temperature before printing. (C) Example of 3D construct printed with hydroxyapatite-rich composite hydrogel. (D) 405nm laser adapter for simultaneous printing and crosslinking.

2.7. Development of a Laser Adapter on Hot Tool

The hot tool available when we started these experiments did not have the ability to photocrosslink, and the separate crosslinking tool was a 365nm light. We therefore sought to develop an on-tool laser to enable photocrosslinking while printing. A 405nm laser (200mW, Luck Laser) was chosen as this wavelength does less damage to DNA than the 365nm wavelength [28] and can photocrosslink using the LAP photoinitiator [13,14]. A holder arm was 3D printed in PLA to attach the laser, battery packs and Raspberry Pi Pico (Figure 1D) [27]. This enables the printing of thicker constructs as crosslinking may not be possible after the print is completed.

2.8. Print Settings

The ideal printing pressures and temperatures for the composite hydrogels were determined using a systematic approach where the pressure was gradually increased in increments of 5 psi, while the temperature was increased from 30°C to 37°C at each interval until a continuous filament was achieved.

2.9. Print Fidelity

Print fidelity is defined as the degree to which a bioprinted structure holds its shape [22]. The bioinks were bioprinted into a square zig zag pattern (Figure 2) [13]. The constructs were crosslinked via the above-mentioned procedure and imaged (VHX-7000, Keyence Inc.).

 doi:10.20944/preprints202312.2084.v1

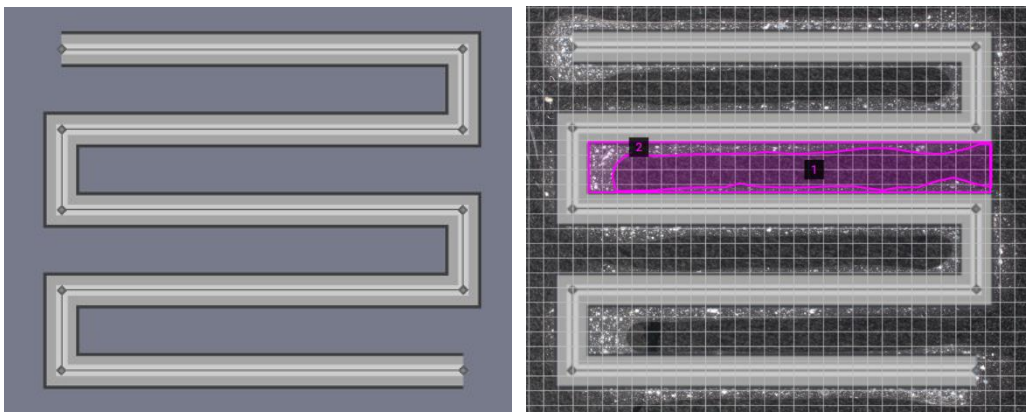

Figure 2. CAD Model used for Print Fidelity. A) Square Zig Zag pattern of length 8.9mm, width 10.9mm, and line thickness of ~.9mm using TSIM. B) Example of an overlaid image with areas of the actual print (1) and theoretical pore size (2) delineated.

Photographs were taken and overlayed onto the TSIM model. The area was measured using an area calculator [29]. These measurements were used to calculate the print fidelity according to the equation below, where $\mathbf{A_{th}}$ is the theoretical pore area and $\mathbf{A_e}$ is the experimental pore area. A value of 100% is perfect print fidelity, a value below 100% indicates underprinting, and a value above 100% represents overprinting.

$$\textbf{Equation 1: Print Fidelity } (\%) = \frac{A_{th}}{A_e}\ x\ 100$$

2.10. Viability

Viability testing was performed using a LIVE/DEAD Viability/Cytotoxicity Kit (ThermoFisher Inc.). Bioinks were both pipetted and printed onto a well plate in triplicate. The bioinks were crosslinked and incubated in growth medium for 2 days and 7 days at 37 °C and 5% CO_2. After each time point, growth medium was removed, and the constructs were washed in PBS. A solution containing 2μM Calcein AM (Invitrogen) and 4 μM Ethidium homodimer-1 (Invitrogen) in PBS was added to the wells and incubated for 25 minutes at 37 °C and 5% CO_2. The dye was then removed, and PBS was added to the wells. The constructs were then imaged and overlayed (Keyence BZ-X810 Microscope). The images were processed and analyzed using the ImageJ/Fiji software with the Stardist plugin.

2.11. Statistical analysis

The design space covered by the DoE combinations was analyzed (StatEase). The z-axis is the standard error of design, and the x/y-axes are GelMA/HA concentrations as pictured (Figure 3). Following testing, ANOVA was performed using the DoE software to demonstrate the effects of GelMA and HA concentrations on the equilibrium modulus and printability and the overall fit of the data to the model. Based on the compression and printability results, we used the DoE software to determine the ideal concentrations of GelMA and HA to optimize mechanical strength. The constraints used were that GelMA had to lie between 5 and 15%, HA between 1 and 33%, pipetability was targeted to be = 0.999 (as close to 1 as possible) with a lower limit of 0.8, and the goal to maximize the equilibrium modulus with a lower limit of 160 kPa and upper limit of 354 kPa.

 doi:10.20944/preprints202312.2084.v1

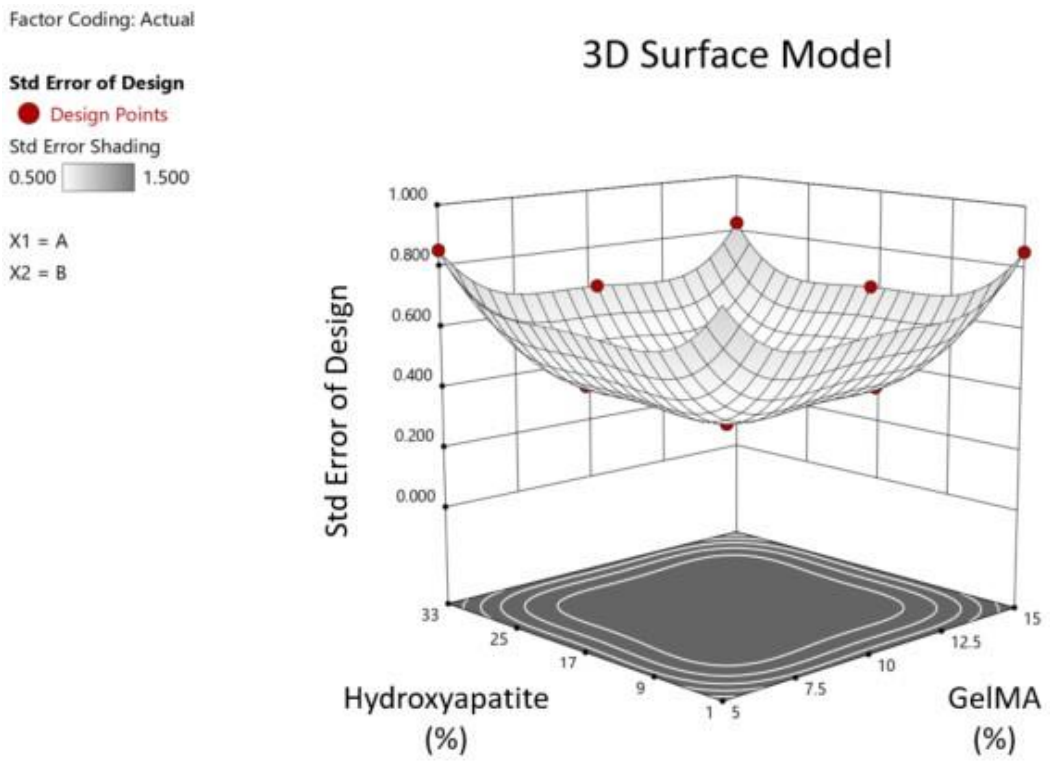

Figure 3. DoE Surface Model. Showing the standard error of design.

Statistical analysis and data illustration for cell viability were performed using GraphPad Prism software. A two-way ANOVA test followed by Sidak's correction for multiple comparisons in the post-hoc test was used to determine statistical significance. Where applicable, data is shown as mean +/- the standard deviation.

3. Results

3.1. Printability of hydrogels

Of the 13 different hydrogels examined, four were unprintable. G10H33, G12.5H25, G15H17 and G15H33 had chalky appearances and did not stay in suspension well. None could be homogenously pipetted at 37°C and were therefore deemed not printable (Figure 4).

 doi:10.20944/preprints202312.2084.v1

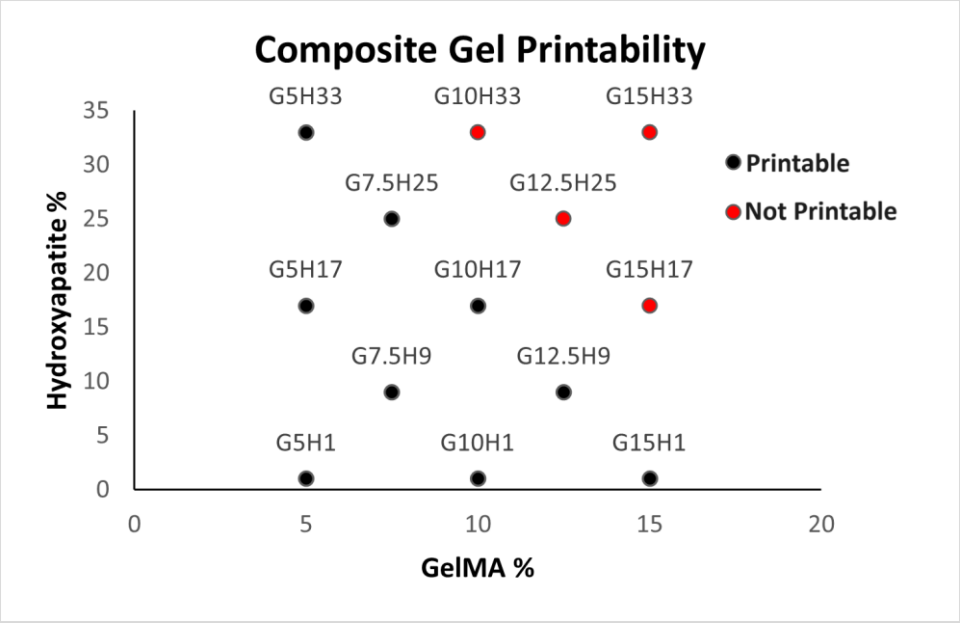

Figure 4. Printability of Composite Hydrogels. G10H33, G12.5H25, G15H17, and G15H33 were not printable, nor could they be pipetted under 37°C. All other hydrogels were both extrudable and printable.

3.2. Mechanical Properties

Mechanical testing showed a positive correlation between both GelMA and HA concentrations and the equilibrium modulus (Figure 5).

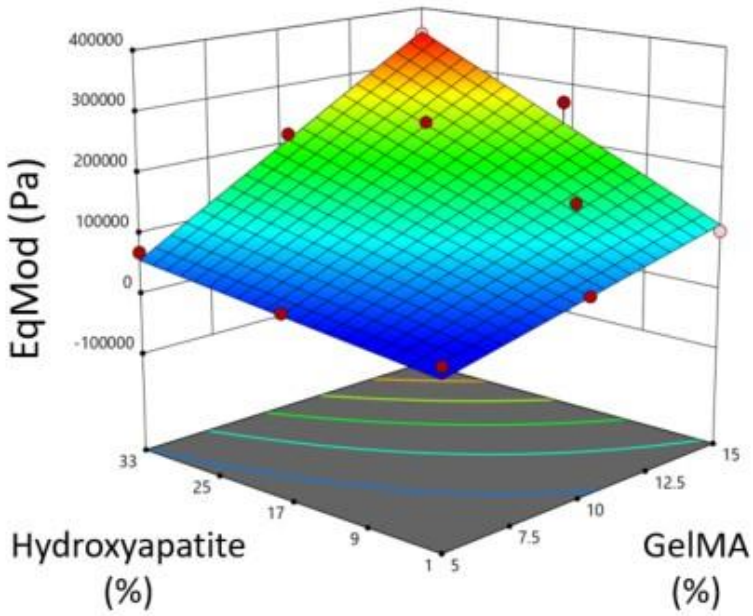

Figure 5. 3D Surface model of compression results. Higher GelMA and HA % corresponded to higher equilibrium moduli.

DoE ANOVA analysis indicated that the augmented 3 level factorial design used was a good fit ($p < 0.0001$). The GelMA, HA, and the combination of the two were significant factors affecting the equilibrium modulus ($p < 0.0001$). Using that data, we used the DoE software to determine that a

 doi:10.20944/preprints202312.2084.v1

composite hydrogel consisting of 12.3116% GelMA, 15.7181% HA, and 2% Gelatin (Gel 1) would produce the maximum equilibrium modulus, predicted to be 170 kPa (Table 2). Because Gel 2 was stiffest pipettable gel before DoE optimization, it was also chosen for further testing. Gel 3 is the bioink used by Allen et al. with the highest HA concentration (Table 2). Moving forward we used the predicted ideal (Gel 1) vs. screen best (Gel 2) vs. literature-based control (Gel 3).

Table 2. GelMA/HA Hydrogels for further testing.

	Gel 1	**Gel 2**	**Gel 3**
GelMA %	12.3116	12.5	10
HA%	15.7181	9	2
Gelatin %	2	2	5
Crosslink time	60s	60s	60s
Experimentally determined Equilibrium Modulus (kPa)	169.895	145.665	58.166

3.3. Print Settings and Print fidelity

3.3.1. Print settings

The ideal extrusion pressure and temperature for the three composite hydrogels were determined qualitatively. The print setup was essentially the same for all three gels (Figure 6A). The collection plate was heated to 35 ℃. All gels produced a continuous filament at two temperature/pressure settings (Figure 6B). As expected, higher temperatures and pressures were required to produce a continuous filament in the hydrogels with higher GelMA and HA concentrations (Figure 6B). Increased printing pressure or temperature beyond this point resulted in over extrusion in all three hydrogels.

3.3.2. Print fidelity

With increasing hydroxyapatite concentration, the materials qualitatively increased in opacity (Figure 6C). All 3 gels were overprinted compared to the CAD model. While no direct relationship between print fidelity and GelMA or HA concentrations was observed, Gel 3 produced the best print fidelity at 155.23% (Figure 6C). Gel 2 produced a pattern with the most over extrusion with a print fidelity 234.14%. It is predicted that the print fidelity is more a reflection of ideal print settings rather than the composition of the gel. The more ideal and precise the settings, the higher the print fidelity.

 doi:10.20944/preprints202312.2084.v1

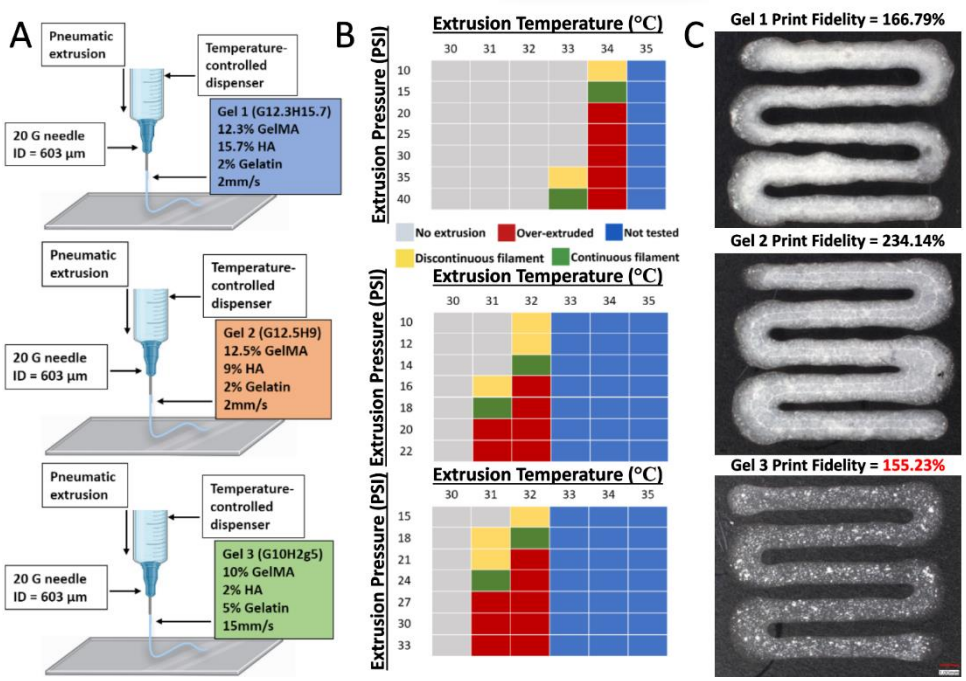

Figure 6. Printability and Print Fidelity of GelMA/HA Composite Hydrogels: (A) Extrusion bioprinting process and the contents of each bioink. Created with Biorender. (B) Determinations of print settings for extrusion of a continuous filament. (C) Images of printed lines with each Gel (Keyence VHX-7000Microscope). Gel 3 produced the highest print fidelity. Scale bar = 1 mm.

3.4. Viability

All gels showed acceptable cell viability. There was significantly higher cell viability in pipetted gel 2 and 3 when compared to both the pipetted and printed gel 1 ($p < 0.05$). Live/Dead staining demonstrated that higher HA concentrations or the higher pressures needed to extrude gel 1 may be cytotoxic to hMSCs (Figure 7A). In addition, there was no significant difference between the same hydrogels at different times ($p > 0.05$).

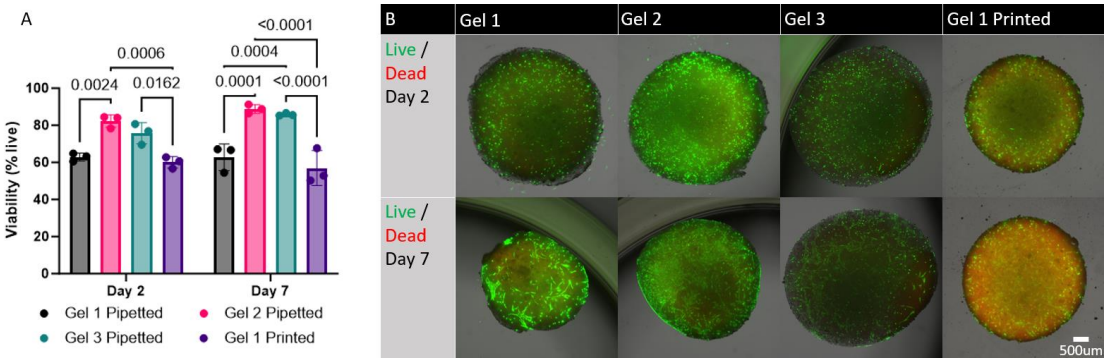

Figure 7. – Cell viability in GelMA/HA bioinks: (A) hMSC viability in each of the 3 gels at day 2 and day 7. Gel 2 and 3 showed significantly higher cell viability as compared to Gel 1. There was no difference between pipetted and printed cell viability in Gel 1. There was also no difference in cell viability from day 2 to day 7 in any gel. (B) Live hMSC cells stained green and dead hMSC cells stained red, composite images are shown.

 doi:10.20944/preprints202312.2084.v1

3. Discussion

An initial screen of hydrogel mixtures was used to make a DoE prediction for the stiffest printable gel. We successfully achieved a well correlated prediction with Gel 1, composed of 12.3% GelMA, 15.7% hydroxyapatite, and 2% gelatin giving an equilibrium modulus ~170 kPa vs. predicted 170 kPa. Gel 2, composed of 12.5% GelMA, 9% hydroxyapatite, and 2% gelatin had a slightly lower equilibrium modulus (~146 kPa) but yielded significantly higher cell viability (~82%) vs. Gel 1 (~60%). Gel 3, composed of 10% GelMA, 2% hydroxyapatite, and 5% gelatin had the highest print fidelity. Thus, we have achieved an increase in the mineral content of bioink to 9% HA vs. 2% in Gel 3 with good viability. However, native bone has a mineral content of ~60-80% [8] so we fall significantly short of that target. It is expected that this scaffold would increase in mineralization with time either in culture or in vivo [30].

Cell viability decreases at temperatures above 37 ℃, thus a cutoff of 37 ℃ was chosen for printability. If a gel is not printable at 37 ℃ or below, it cannot sustain cell viability. It was also found that at temperatures above 37℃, the hydrogels slowly weaken (i.e. lose compressive moduli, data not shown), capping the max temperature at 37℃.

There are multiple possible explanations for the drop in printability at high HA concentrations. For example, high amounts of HA may not have remained suspended within the hydrogels, which then formed a plug at the bottom of the syringe preventing extrusion.

Bone has the greatest stiffness of any tissue in the human body and can sustain immense amounts of pressure. As previously mentioned, the young's modulus of cortical and trabecular bone is ~19.9 GPa and ~18.0 GPa, respectively [9]. While this number may be impossible to achieve using hydrogels, a 3D bioprinted bone construct with an equilibrium modulus >64 kPa was achieved, making it similar to the hardness of the pre-calcified bone matrix [10]. In addition, the hMSCs may increase the hardness of the material over time due to the release of osteogenic molecules that increase mechanical stiffness [29].

The increasing opacity of high % HA may have also affected the mechanical stiffness by preventing the laser from fully penetrating the material, creating non-uniform crosslinking. This was addressed by simultaneously printing and crosslinking. One drawback to this is that each part of the gel is only crosslinked for a moment as the laser passes through.

The two print settings that were quantified were temperature and pressure (Figure 6B). Both had a significant effect on the quality of the extruded filament. As expected, hydrogels containing higher GelMA and HA concentrations required a higher temperature and pressure to achieve a continuous filament. One of the challenges when heating the gel within the printer was a potential lack of uniformity of temperature within the tube itself. This resulted in regions of varying temperature and while printing resulting in some patterns of over-extrusion followed by under-extrusion. The temperature near the tip of the heated syringe was also likely lower as it was outside of the heating apparatus. As a result, higher pressures were needed in order to start extrusion and then the pressure would be lowered to maintain the print. Another factor that was less optimized was the print speed and bed temperature, which can have a significant effect on the fidelity.

Print fidelity is crucial for assessing the ability of a bioink to be engineered for patient-specific implants and depends on many factors such as gelation time, temperature, print speed and pressure. Bioinks with high print fidelity will produce a value close to 100%, meaning they hold their shape to a significant degree. Bioinks with greater than 100% print fidelity will be overprinted and collapse on the central pore. Bioinks with lower than 100% print fidelity will be underprinted and produce a central pore area that is larger than that of the model.

With the print settings shown in Figure 6B, Gel 3 produced the most optimal print fidelity. Although all three gels produced constructs that qualitatively modeled the computer aided design, all were slightly overprinted. While some of the print fidelity results can be attributed to the characteristics of the gel, it is difficult to determine the degree to which the bioink itself influences print fidelity. The material concentrations influence the time required for the material to become a solid after printing. However, this effect could be controlled by performing photocrosslinking during the bioprinting process. Gelation time, temperature, print speed and pressure can all heavily

 doi:10.20944/preprints202312.2084.v1

influence print fidelity. It is likely that with more precise control over temperature and pressure, and with immediate photocrosslinking, all 3 gels could produce a more optimal print fidelity. Therefore, although Gel 3 produced the print fidelity closest to 100%, this may not mean that it is significantly better at modeling the computer aided design than Gel 1 or Gel 2. Despite these limitations, we determined that Gel 3 performed the best with the print settings shown in Figure 6B.

All three materials sustained adequate cell viability, indicating that hMSCs can survive within the hydrogels through the photocrosslinking process. The results also showed that all three hydrogels can sustain hMSC viability for at least 7 days in culture. Increasing concentrations of HA may have affected cell viability in gel 1 which had an HA concentration of 15.7%. This is significantly higher than the highest HA concentration previously tested in the literature, which was 2% HA [16]. We predicted that a printed gel may have lower cell viability as a result of high extrusion pressures. This however was not the case as the cell viability in printed gel 1 was not significantly different from pipetted gel 1. Cell viability did not change with intermittent pressures of up to 40psi. Of the three gels tested, Gel 2 seemed to exhibit a trend toward consistently higher viability, but this difference was not statistically significant when compared to gel 3. These results indicate that although all three hydrogels are suitable for sustaining hMSCs for an extended period, gel 2 may be the most optimal given the combination of stiffness and viability for 3D bioprinted bone implants.

The cell viability in printed gel 1 did not change significantly when compared to pipetted gel 1. Analysis of viability in printed gel 2 and gel 3 was not possible because the data was not quantifiable (Supplemental Figure 1). Given that the higher pressure necessary to extrude gel 1 (20 psi vs 14-18 psi for gels 2 and 3) did not seem to significantly affect viability, cell viability likely would not have been different when comparing printed and pipetted gel 2 and 3.

4. Conclusion

3DBP is a promising alternative to the current gold standard for the regeneration of critical sized bone defects. The ideal bioink to produce bone-like tissue should be one that is easily printable and maintains adequate mechanical strength while sustaining cell viability for *in vivo* ossification. While the ideal materials for this bioink have yet to be discovered, the results of this study demonstrate that hydrogels combining GelMA and HA are suitable materials for 3DBP of bone-like constructs and have promising future implications as 3D bioprinted bone substitutes. This research showed that a GelMA/HA bioink consisting of 12.3% GelMA, 15.7% HA, and 2% Gelatin would produce the greatest mechanical stiffness, and a hydrogel consisting of 10% GelMA, 2% HA, and 5% Gelatin produced the best print fidelity. A gel composed of 12.5% GelMa, 9% HA, and 2% Gelatin, however, would likely be the most ideal candidate for further research because of its high equilibrium modulus and its increased viability when compared to gel 1. However, more research is required to determine if GelMA/HA constructs can match the hardness of physiological bone after time in culture, and if the constructs promote regeneration of critical sized defects in animal models. Bioinks containing these concentrations of GelMA and HA should be considered in the development of future 3DBP bone implants for reconstruction of complex defects.

Author Contributions: Conceptualization: T.K., J.D., K.M.; Methodology: T.K., J.D., K.M.; Formal analysis: P.S., T.K.; Investigation: P.S., S.S, L.M.; Data curation: P.S., T.L.; Writing—original draft preparation: P.S., J.D; Writing—review and editing: P.S., T.K.; Supervision: T.K., K.M.; Project administration: T.K.; All authors have read and agreed to the published version of the manuscript.

Funding: Funding was provided by the University of Central Florida and the University of Central Florida College of Medicine.

Institutional Review Board Statement: The human mesenchymal stromal cells used in this study were approved for use in non-human research under IRB-approved protocols (University of Central Florida College of Medicine STUDY00001124).

Data Availability Statement: The raw/processed data generated in this work are available upon request from the corresponding author.

Conflicts of interest: The authors declare that they do not have any known competing financial interests or personal relationships that could have influenced the work in this study.

References

1. A. H. Schmidt, "Autologous bone graft: Is it still the gold standard?," (in eng), *Injury,* vol. 52 Suppl 2, pp. S18-s22, Jun 2021, doi: 10.1016/j.injury.2021.01.043.
2. I. Roohani, G. C. Yeo, S. M. Mithieux, and A. S. Weiss, "Emerging concepts in bone repair and the premise of soft materials," (in eng), *Curr Opin Biotechnol,* vol. 74, pp. 220-229, Apr 2022, doi: 10.1016/j.copbio.2021.12.004.
3. S. C. Darveau *et al.*, "Existing clinical evidence on the use of cellular bone matrix grafts in spinal fusion: updated systematic review of the literature," (in eng), *Neurosurg Focus,* vol. 50, no. 6, p. E12, Jun 2021, doi: 10.3171/2021.3.Focus2173.
4. L. Roseti *et al.*, "Scaffolds for Bone Tissue Engineering: State of the art and new perspectives," (in eng), *Materials science & engineering. C, Materials for biological applications,* vol. 78, pp. 1246-1262, Sep 1 2017, doi: 10.1016/j.msec.2017.05.017.
5. A. GhavamiNejad, N. Ashammakhi, X. Y. Wu, and A. Khademhosseini, "Crosslinking Strategies for 3D Bioprinting of Polymeric Hydrogels," (in eng), *Small (Weinheim an der Bergstrasse, Germany),* vol. 16, no. 35, p. e2002931, Sep 2020, doi: 10.1002/smll.202002931.
6. T. J. Kean and M. Thanou, "Utility of Chitosan for 3D Printing and Bioprinting," in *Sustainable Agriculture Reviews 35: Chitin and Chitosan: History, Fundamentals and Innovations*, G. Crini and E. Lichtfouse Eds. Cham: Springer International Publishing, 2019, pp. 271-292.
7. R. L. Pan *et al.*, "Systematic review on the application of 3D-bioprinting technology in orthoregeneration: current achievements and open challenges," *J Exp Orthop,* vol. 9, no. 1, p. 95, Sep 19 2022, doi: 10.1186/s40634-022-00518-3.
8. T. Genova, I. Roato, M. Carossa, C. Motta, D. Cavagnetto, and F. Mussano, "Advances on Bone Substitutes through 3D Bioprinting," vol. 21, no. 19, p. 7012, 2020, doi: 10.3390/ijms21197012.
9. H. H. Bayraktar, E. F. Morgan, G. L. Niebur, G. E. Morris, E. K. Wong, and T. M. Keaveny, "Comparison of the elastic and yield properties of human femoral trabecular and cortical bone tissue," (in eng), *J Biomech,* vol. 37, no. 1, pp. 27-35, Jan 2004, doi: 10.1016/s0021-9290(03)00257-4.
10. L. Parmentier, M. Riffault, and D. A. Hoey, "Utilizing Osteocyte Derived Factors to Enhance Cell Viability and Osteogenic Matrix Deposition within IPN Hydrogels," vol. 13, no. 7, p. 1690, 2020. [Online]. Available: https://www.mdpi.com/1996-1944/13/7/1690.
11. M. Akhmanova, E. Osidak, S. Domogatsky, S. Rodin, and A. Domogatskaya, "Physical, Spatial, and Molecular Aspects of Extracellular Matrix of In Vivo Niches and Artificial Scaffolds Relevant to Stem Cells Research," *Stem Cells International,* vol. 2015, p. 167025, 2015/08/16 2015, doi: 10.1155/2015/167025.
12. S. Naghieh, M. R. Karamooz-Ravari, M. D. Sarker, E. Karki, and X. Chen, "Influence of crosslinking on the mechanical behavior of 3D printed alginate scaffolds: Experimental and numerical approaches," *Journal of the Mechanical Behavior of Biomedical Materials,* vol. 80, pp. 111-118, 2018/04/01/ 2018, doi: 10.1016/j.jmbbm.2018.01.034.
13. K. Martyniak *et al.*, "Optimizing Bioink Composition for Human Chondrocyte Expression of Lubricin," *Bioengineering,* vol. 10, no. 9, p. 997, 2023. [Online]. Available: https://www.mdpi.com/2306-5354/10/9/997.
14. K. Martyniak, A. Lokshina, M. A. Cruz, M. Karimzadeh, R. Kemp, and T. J. Kean, "Biomaterial composition and stiffness as decisive properties of 3D bioprinted constructs for type II collagen stimulation," *Acta Biomaterialia,* 2022/08/29/ 2022, doi: https://doi.org/10.1016/j.actbio.2022.08.058.
15. J. Yin, M. Yan, Y. Wang, J. Fu, and H. Suo, "3D Bioprinting of Low-Concentration Cell-Laden Gelatin Methacrylate (GelMA) Bioinks with a Two-Step Cross-linking Strategy," (in eng), *ACS applied materials & interfaces,* vol. 10, no. 8, pp. 6849-6857, Feb 28 2018, doi: 10.1021/acsami.7b16059.
16. N. B. Allen, B. Abar, L. Johnson, J. Burbano, R. M. Danilkowicz, and S. B. J. B. Adams, "3D-bioprinted GelMA-gelatin-hydroxyapatite osteoblast-laden composite hydrogels for bone tissue engineering," *Bioprinting,* vol. 26, p. e00196, 2022.
17. C. Colosi *et al.*, "Microfluidic Bioprinting of Heterogeneous 3D Tissue Constructs Using Low-Viscosity Bioink," (in eng), *Advanced materials (Deerfield Beach, Fla.),* vol. 28, no. 4, pp. 677-84, Jan 27 2016, doi: 10.1002/adma.201503310.
18. Y. Zuo *et al.*, "Photo-cross-linkable methacrylated gelatin and hydroxyapatite hybrid hydrogel for modularly engineering biomimetic osteon," *ACS Appl Mater Interfaces,* vol. 7, no. 19, pp. 10386-94, May 20 2015, doi: 10.1021/acsami.5b01433.
19. S. Suvarnapathaki, X. Wu, D. Lantigua, M. A. Nguyen, and G. Camci-Unal, "Hydroxyapatite-Incorporated Composite Gels Improve Mechanical Properties and Bioactivity of Bone Scaffolds," *Macromol Biosci,* vol. 20, no. 10, p. e2000176, Oct 2020, doi: 10.1002/mabi.202000176.

20. A. Wenz, K. Borchers, G. E. M. Tovar, and P. J. Kluger, "Bone matrix production in hydroxyapatite-modified hydrogels suitable for bone bioprinting," (in eng), *Biofabrication,* vol. 9, no. 4, p. 044103, Nov 14 2017, doi: 10.1088/1758-5090/aa91ec.
21. S. Mansour, S. El-dek, M. Ismail, M. J. B. P. Ahmed, and E. Express, "Structure and cell viability of Pd substituted hydroxyapatite nano particles," *Biomed Phys Eng Express,* vol. 4, no. 4, p. 045008, 2018.
22. A. Schwab, R. Levato, M. D'Este, S. Piluso, D. Eglin, and J. Malda, "Printability and Shape Fidelity of Bioinks in 3D Bioprinting," (in eng), *Chemical reviews,* vol. 120, no. 19, pp. 11028-11055, Oct 14 2020, doi: 10.1021/acs.chemrev.0c00084.
23. S. Bose, S. Vahabzadeh, and A. J. M. t. Bandyopadhyay, "Bone tissue engineering using 3D printing," *Materials today,* vol. 16, no. 12, pp. 496-504, 2013.
24. J. F. Weber and S. D. Waldman, "Chapter 21 - In Situ and Ex Vivo Biomechanical Testing of Articular Cartilage," in *Experimental Methods in Orthopaedic Biomechanics*, R. Zdero Ed.: Academic Press, 2017, pp. 331-347.
25. N. Ashammakhi *et al.*, "Advancing frontiers in bone bioprinting," *Adv Healthcare Mater* vol. 8, no. 7, p. 1801048, 2019.
26. K. Martyniak *et al.*, "Optimizing bioink composition for human chondrocyte expression of lubricin," p. 2022.11. 14.516490, 2022.
27. Y. Kang, S. Kim, J. Bishop, A. Khademhosseini, and Y. Yang, "The osteogenic differentiation of human bone marrow MSCs on HUVEC-derived ECM and β-TCP scaffold," (in eng), *Biomaterials,* vol. 33, no. 29, pp. 6998-7007, Oct 2012, doi: 10.1016/j.biomaterials.2012.06.061.
28. M. Klak *et al.*, "Irradiation with 365 nm and 405 nm wavelength shows differences in DNA damage of swine pancreatic islets," *PLoS One,* vol. 15, no. 6, p. e0235052, 2020, doi: 10.1371/journal.pone.0235052.
29. C. S. Linsley, B. M. Wu, and B. Tawil, "Mesenchymal stem cell growth on and mechanical properties of fibrin-based biomimetic bone scaffolds," vol. 104, no. 12, pp. 2945-2953, 2016, doi: https://doi.org/10.1002/jbm.a.35840.
30. D. Bakkalci, A. Micalet, R. Al Hosni, E. Moeendarbary, and U. Cheema, "Associated changes in stiffness of collagen scaffolds during osteoblast mineralisation and bone formation," (in eng), *BMC Res Notes,* vol. 15, no. 1, p. 310, Sep 24 2022, doi: 10.1186/s13104-022-06203-z.